International Journal of Innovative Research and Scientific Studies, 8(6) 2025, pages: 1930-1940

IJIRSS
International Journal of Innovative Research & Scientific Studies

ISSN: 2617-6548

URL: www.ijirss.com

Effective surface residual stress in diamond burnishing 18/8 austenitic stainless steels

Mariana Ichkova[1,2]

[1]*Department of Material Science and Mechanics of Materials, Technical University of Gabrovo, 5300 Gabrovo, Bulgaria.*
[2]*Center of competence "Smart mechatronic, eco-and energy-saving systems and technologies", Technical University of Gabrovo, 5300 Gabrovo, Bulgaria.*

(*Email: ichkova@tugab.bg*)

Abstract

Diamond burnishing (DB) 18/8 chromium-nickel austenitic stainless steel (CNASS) introduces a two-phase (austenite and strain-induced martensite) surface-layer structure. Residual stress measurements using X-ray diffraction separately for the two phases result in different outcomes due to the difference in elastic constants. The concept of effective surface residual stress (ESRS) was introduced in this study to solve this problem. The ESRS is the sum of the measured residual stresses for the two phases, multiplied by the respective weighting factors corresponding to the percentage of content of the two phases. Thus, the inhomogeneous surface (under the phase composition criterion) is homogenized, and the ESRS is an integral characteristic of this homogenized surface. The primary objective is to establish the influence of the DB governing factors on the ESRS in diamond-burnished 18/8 CNASS. This study employs an X-ray technique, planned experiment, regression analysis, and analysis of variance. A mathematical model of the ESRS was created. The burnishing velocity has the most influence on ESRS, followed by the feed rate and burnishing force. The DB method produces two effects: mechanical and thermal. Combinations of various magnitudes of the governing factors change the ratio between these effects, leading to different magnitudes of ESRS. The feed rate affects ESRS unidirectionally (increasing the feed rate decreases ESRS) because the feed rate does not create a thermal effect. Conversely, the burnishing force and velocity influence the mechanical and thermal effects created by DB. The ESRS depends on the percentage of induced martensite to a greater extent than surface microhardness.

Keywords: Chromium-nickel austenitic stainless steel, Diamond burnishing, Effective surface residual stress, Strain-induced martensite.

DOI: 10.53894/ijirss.v8i6.10046
Funding: This research was funded by the European Regional Development Fund under the Operational Program "Scientific Research, Innovation and Digitization for Smart Transformation 2021–2027", Project CoC "SmartMechatronics, Eco- and Energy Saving Systems and Technologies", BG16RFPR002-1.014-0005.
History: Received: 30 July 2025 / **Revised:** 1 September 2025 / **Accepted:** 4 September 2025 / **Published:** 19 September 2025

Competing Interests: The author declares that there are no conflicts of interests regarding the publication of this paper.
Transparency: The author confirms that the manuscript is an honest, accurate, and transparent account of the study; that no vital features of the study have been omitted; and that any discrepancies from the study as planned have been explained. This study followed all ethical practices during writing.
Publisher: Innovative Research Publishing

1. Introduction

Increasing the share of stainless steels, 70% of which are austenitic, is a sustainable modern steelmaking trend [1]. Although manganese and nitrogen also extend the austenitic region to room temperature, the vast majority of austenitic steels are chromium-nickel due to their favorable combination of properties: superior general corrosion resistance, good machinability and weldability, and workability in a wide temperature range (up to 450°C). Moreover, 18/8 chromium-nickel austenitic stainless steels (CNASSs; approximately 18 wt% chromium and 8 wt% nickel) are the most common due to their minimal nickel content, making them the least expensive.

Austenite is the softest phase in iron-carbon alloys. Various approaches can increase the hardness and strength of CNASS, among which the least expensive is surface cold working (static or dynamic) based on severe surface plastic deformation. Dynamic methods are based on the effect of deforming elements (spheres with a diameter of several tenths of millimeters to several millimeters) on the treated surface. The process is stochastic, but the resulting roughness is unsatisfactory [2]. Static surface cold working (i.e., burnishing) is realized by employing a hard, smooth, deforming element pressed with a constant static force normal to the worked surface, which moves relative to it. Thus, this approach decreases roughness, increases microhardness, introduces residual compressive stresses, and changes the grain shape and size [3].

According to the type of tangential contact between the deforming element and processed surface, burnishing methods are classified into two groups. In the first group, the deforming element (sphere or roller) rolls without slipping, and the methods are called ball or roller burnishing [4, 5]. In the second group, a spherical- or cylindrical-ended deforming element slides along the machined surface; hence, the method is called slide burnishing [6].

When the deforming element is a natural or synthetic diamond, the method is called diamond burnishing (DB) [7]. The diamond is the hardest mineral according to the 10-degree Mohs scale, allowing DB to process even the hardest alloys. In addition, DB is realized using significantly simpler equipment compared to the first group of methods. Thus, DB has been established as an inexpensive and effective finishing method for structural [8-12] tools [13-15] stainless [16-19] steels, and nonferrous alloys [20, 21]. Furthermore, DB is a preferred method for implementing hybrid [22, 23] and combined processes [23-25].

Extensive studies of the effects of DB on the surface integrity (SI) and operational behavior (fatigue, wear, and corrosion) of CNASS have been conducted [3, 16, 18, 19, 25-28]. In addition, DB causes severe plastic deformation of the surface layers of CNASS, causing part of the austenite in this layer to transform into α'-martensite when the nickel content in the steel is below 15 wt% [16]. Austenite is stable when the nickel content is above 15 wt%, as nickel reduces the ability of austenite to strain-harden. When the CNASS must satisfy a requirement for a high degree of strain-hardening, the nickel content is limited to 8 to 9 wt% [16].

Moreover, DB can form two phases of strain-induced martensite: α' and ε. The second phase is a consequence of the smaller plastic deformations and transforms into the α'-phase when the degree of plastic deformation increases [29]. As a harder phase, α'-martensite increases the microhardness [16] but worsens the resistance to electrochemical corrosion [3]. Additionally, α'-martensite is metastable, and after increasing the temperature, the reverse transformation is observed ($\alpha' \rightarrow \gamma$) [16].

Very few studies have assessed the effect of surface cold working on the $\gamma \rightarrow \alpha'$ phase transformation [16, 30, 31]. The percentages of martensite in the surface and subsurface layers are necessary to determine the residual stresses in CNASS correctly, using the X-ray method to select elastic constants and measure the residual stress distribution. The residual compressive stresses introduced via surface cold working delay the formation of fatigue macrocracks in the metal component, increasing the fatigue strength. Thus, knowledge of the residual stress distribution in CNASS components enables the prediction of the fatigue life of the respective metal components.

The residual stresses can be measured via X-ray using the elastic constants of the austenitic or martensitic phases. If induced α'-martensite is absent, the measurement for the austenitic phase would be correct and representative of the respective component. Conversely, with a high degree of plastic deformation of 18/8 CNASS, if the α'-martensite content in the surface layer is 100%, the measurement of residual stresses for the martensitic phase would be correct. The induced α'-martensite is most significant in the surface layer, and at a depth of about 0.1 mm, it rapidly decreases to 0 [16]. However, the problem is how to proceed if the two phases (austenitic and martensitic) are equivalent in percentage of content, which primarily occurs on the surface.

The concept of effective surface residual stress (ESRS) is introduced in this study to solve this problem. The ESRS is the sum of the measured residual stresses for the two phases, multiplied by the respective weighting factors corresponding to the percentage of content of these two phases. Thus, the inhomogeneous surface (according to the phase composition criterion) is homogenized, and the ESRS is a characteristic of this homogenized surface.

The primary objective is to establish the influence of the governing factors of the DB process on the ESRS in diamond-burnished 18/8 CNASS. The present study is a continuation of previous work [32] dedicated to the influence of the governing factors of DB of AISI 304 steel on height and shape roughness parameters.

2. Materials and Methods

The AISI 304 CNASS was obtained as hot-rolled bars with a diameter of 16 mm and was used in the as-received state. The chemical composition was established using an optical emission spectrometer. Tensile tests at room temperature were conducted via the Zwick/Roell Vibrophore 100 testing machine. The tensile test specimen geometry is provided by ISO 6892-1:2019 [33]. The material hardness was measured using a VEB-WPM tester with a spherical-ended indenter with a diameter of 2.5 mm, loading of 63 kg, and holding time of 10 s.

Further, DB was implemented on an Index Traub CNC lathe using conventional flood lubrication. Figure 1 presents the kinematic scheme with governing factors and the burnishing devices. The burnishing devices provide elastic normal contact between the deforming element and treated surface.

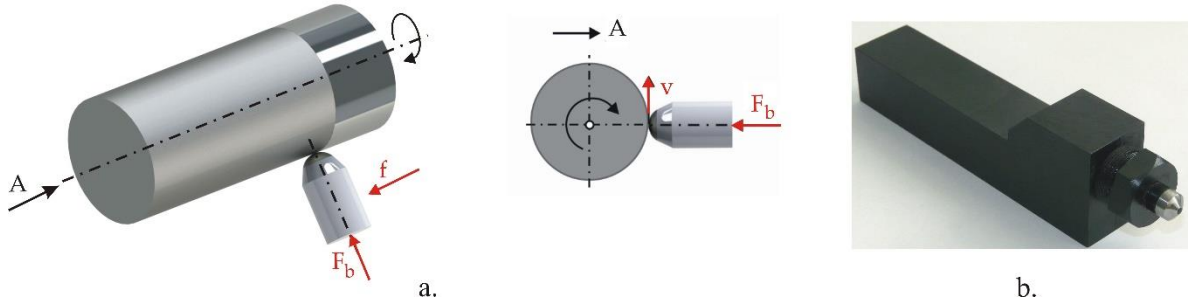

Figure 1.
DB implementation: a. kinematics and governing factors; b. DB device.

Previous turning and DB were conducted in one clamping process to minimize the concentric run-out in DB. This experiment employed a VCMT 160404-F3P carbide cutting insert (main back angle $\alpha_0 = 7^o$; tool-tip radius = 0.4 mm) for turning. Moreover, this work employed an SVJCR 2525M-16 holder with main and auxiliary setting angles of $\chi_c = 93^o$ and $\chi_c = 52^o$, respectively. In addition, ISCAR Bulgaria manufactured the cutting insert and holder. The average value of the Ra roughness parameter after the previous turning was 0.529 μm.

A Bruker D8 ADVANCE diffractometer with a pin-hole collimator, a primary beam measuring 1x1 mm, and the specialized software DIFFRAC.Dquant V1.5 [34] were employed to measure the percentage of content on the surface of the two phases (austenitic and α'-martensitic) and the residual surface stresses. The $\sin^2\psi$ method with the least-squares fitting procedure evaluated the residual stresses. Table 1 presents detailed information on the residual stress measurement.

Table 1.
Characteristics of the residual stress X-ray measurement.

Measuring device	**Bruker D8 Advance diffractometer**
X-ray tube	Long focus Cr – Kα
Crystallographic planes	Fe(γ) – (220); Fe(α) – (211)
Diffraction angle (2θ)	128.78° (124° … 133°)
Measuring method	Offset coupled TwoTheta/Theta ($\sin^2\psi$ method)
Scan mode	Continuous PSD fast
X-ray detector	SSD160-2 (1D scanning)
Collimator spot size	Standard Φ1.0 mm
Measurement time for single scan	Approx. 35 s
Elastic constant s1 (austenite)	$-1.352\ \text{TPa}^{-1}$
Elastic constant 1/2s2 (austenite)	$6.182\ \text{TPa}^{-1}$
Elastic constant s1 (martensite)	$-1.271\ \text{TPa}^{-1}$
Elastic constant 1/2s2 (martensite)	$5.811\ \text{TPa}^{-1}$
Voltage	30 kV
Current	40 mA
Step size	0.5
Time for step	1 s

The surface axial residual stress values were measured because they have a greater influence on fatigue behavior compared to circumferential stress. The ESRS was calculated using the following formula:

$$\sigma_{eff} = \alpha\sigma^{aust} + \beta\sigma^{mart} \quad (1)$$

where α and β are weighting coefficients (α + β = 1), corresponding to the percentage of content of the two phases (austenitic and martensitic) in the surface layer, and σ^{aust} and σ^{mart} are the measured surface residual stresses, for the austenitic and martensitic phases, respectively.

The ZHVμ Zwick/Roell microhardness tester (Ulm, Germany) was employed to establish the surface microhardness. The loading and holding times were 0.05 kg and 10 s, respectively. The final surface microhardness value was the center of clustering of 10 measurements.

3. Experimental Results

3.1. AISI 304 Steel in the as-Received State

The chemical composition in weight percent (wt%) is as follows: iron (Fe): 69.51, carbon (C): 0.023, silicon (Si): 0.271, manganese (Mn): 1.6, phosphorus (P): 0.047, sulfur (S): 0.034, chromium (Cr): 19.19, nickel (Ni): 7.98, molybdenum (Mo): 0.243, copper (Cu): 0.637, cobalt (Co): 0.161, vanadium (V): 0.06, tungsten (W): 0.041. Small amounts of titanium (Ti), aluminum (Al), lead (Pb), tin (Sn), niobium (Nb), boron (B), arsenic (As), zinc (Zn), bismuth (Bi), zirconium (Zr), and calcium (Ca) with a total of 0.203 wt% were also detected. The mechanical characteristics of the tested steel are yield limit = 338 MPa, tensile strength = 733 MPa, elongation = 44.7%, and hardness = 250 HB.

3.2. Design

The selected governing factors were the burnishing force F_b, feed rate f, and burnishing velocity v (Figure 1a). Table 2 lists the governing factor magnitudes selected based on the results obtained in previous work [16]. The radius of the spherical-ended polycrystalline diamond insert was 2 mm. According to a previous study [16] this radius magnitude provides the highest degree of surface plastic deformation, with the same values as other governing factors. The upper burnishing force level is 500 N because higher values worsen the resulting roughness [16]. The objective function was the ESRS Y_σ.

Table 2.
Governing factors and levels.

Governing factors	**Levels**							
	Natural, $\tilde{x}_i$				**Coded,** x_i			
Burnishing force F_b [N]	$\tilde{x}_1$	100	300	500	x_1	-1	0	1
Feed rate f [mm / rev]	$\tilde{x}_2$	0.02	0.05	0.08	x_2	-1	0	1
Burnishing velocity v [m/min]	$\tilde{x}_3$	50	85	120	x_3	-1	0	1

A planned experiment and a second-order optimal composition design were employed. The approximating polynomial cannot be higher than the second-order because the governing factors vary at three levels. The experimental points (14 total) are at the vertices of the cubic factor space and the centers of the six faces of the cube. Box and Wilson [35] proposed the optimal composition plans, which are widely used because they allow for the description of the studied phenomenon in a wide range of input variables. Table 3 presents the experimental plan.

Table 3.
Experimental plan.

Experimental point	1	2	3	4	5	6	7	8	9	10	11	12	13	14
Burnishing force x_1	-1	1	-1	1	-1	1	-1	1	-1	1	0	0	0	0
Feed rate x_2	-1	-1	1	1	-1	-1	1	1	0	0	-1	1	0	0
Burnishing speed x_3	-1	-1	-1	-1	1	1	1	1	0	0	0	0	-1	1

3.3. Experimental Results

The average values of the Ra roughness parameter and surface microhardness after turning were $R_a^{init} = 0.529$ μm and 421 HV, respectively. Table 4 presents the results for the percentage of content of the two phases and the residual surface axial stresses, measurement errors, and ESRS, calculated using Equation 1.

The regression analysis of the ESRS results was conducted using QStatLab software [36]. Given the experimental design, the regression model takes the following form:

$$Y_\sigma(\{X\}) = b_0 + \sum_{i=1}^{3} b_i x_i + \sum_{i=1}^{2} \sum_{j=i-1}^{3} b_{ij} x_i x_j + \sum_{i=1}^{3} b_{ii} x_i^2 , \quad (2)$$

where $\{X\}$ denotes the vector of the governing factors x_i, $i = 1,2,3$.

Table 4.
Phase distribution and residual stresses.

Experim. point	**Phase distribution, %**		**Measured residual stresses and errors, MPa**				**Effective stress MPa**
	Austenite	**Martensite**	**Austenite**		**Martensite**		
			Stress	**Error**	**Stress**	**Error**	
1	30.35	69.65	-1124.4	146.1	-1393.1	74.4	-1311.55
2	11.80	88.20	-1089	148.2	-1348.2	82.8	-1317.61
3	91.30	8.70	-900.6	114.6	-1457.7	118.8	-1077.57
4	36.40	63.60	-862	160.3	-1316.2	110.2	-1150.87
5	50.40	49.60	-691.9	146	-1375.6	90.8	-1344.78
6	49.10	50.90	-789.4	236.7	-1261.8	60.7	-1029.85
7	100	0	-968.6	74.8	N.A.	N.A.	-968.60
8	84.70	15.30	-849.3	118.4	-1614.4	186.5	-966.36
9	72.60	27.40	-794.9	91.7	-1413.4	83.1	-964.37
10	64.60	35.40	-473.5	116.7	-1221.2	79.7	-738.18
11	24.00	76.00	-737.9	82.2	-1192.6	82.2	-1083.47
12	74.00	26.00	-392.7	165.6	-1246.6	91.9	-614.71
13	30.30	69.70	-819.4	142.6	-1411.1	90	-1231.81
14	88.10	11.90	-874.5	76.3	-1378.9	113.9	-934.52

Table 5 lists the polynomial coefficients of the Y_σ model. The probability of a coefficient being insignificant is p=0.05. However, all coefficients (excluding b_{23}, which is 0) are included in the models to minimize the residual. The statistical analysis of the Y_σ model was performed using QstatLab. The critical values of the Student statistics (T), Fisher statistics (F), residual standard deviation (Res. sd), determination coefficient (R^2), and adjusted determination coefficient (adj. R^2) [36] are as follows: T=2.57058, F=4.81832, Res. sd=105.72, R^2=0.98582, and adj. R^2=0.95514. The results confirm the adequacy of the Y_σ model.

Table 5.
Regression coefficients of the Y_σ model.

b_{ij}	b_0	b_1	b_2	b_3	b_{11}	b_{22}	b_{33}	b_{12}	b_{13}
Y_σ	-818.816	46.4	130.915	84.53	-32.459	-30.274	-264.35	-47.491	49.566

Figure 2 graphically presents the dependencies of the objective function Y_σ on each pair of variables, with the third variable fixed at an average level. A visual inspection indicates the following results: 1) the feed rate (Figure 2a) and

burnishing velocities (Figure 2b) have a greater influence on Y_σ than the burnishing force, and 2) the burnishing velocity has a greater influence on Y_σ than the feed rate (Figure 2c). Table 6 presents the measured values of the surface microhardness at the experimental points.

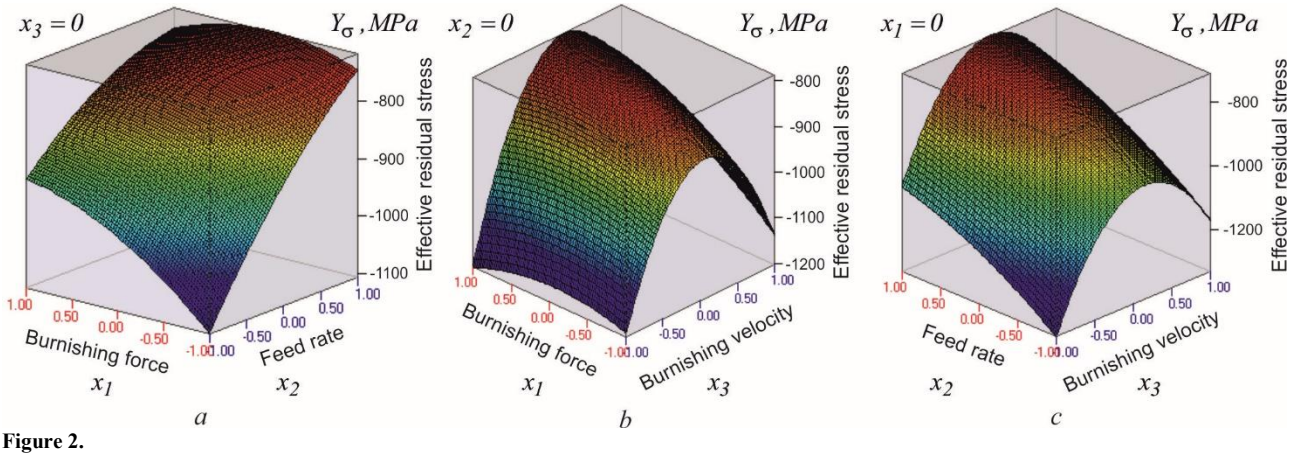

Figure 2.

A graphical representation of the dependencies of the objective function Y_σ on each pair of variables: a. effects of burnishing force and feed rate; b. effects of burnishing force and burnishing velocity; c. effects of feed rate and burnishing velocity.

4. Discussion

The DB method is thermomechanical, which is a consequence of the sliding friction contact between the deforming element and treated surface. The work from the friction and surface plastic deformation dissipates into heat. Over 70% of the internal (input) work is spent on friction in the DB process, whereas the friction dissipation work in ball or roller burnishing is negligible [8]. In addition, the plastic deformation work in the DB process is greater than that for ball and roller burnishing.

The generated heat (i.e., thermal effect in the DB process) leads to a so-called softening effect [37] which increases with an increasing burnishing velocity. The softening effect causes a decrease in microhardness and a reduction in surface residual compressive stresses. In addition, as the generated heat increases, the temperature in the diamond–treated surface contact area also increases. Thus, the phase transformation $\gamma \rightarrow \alpha'$ is suppressed, and α'-martensite is a metastable phase. With increasing temperature, the formed α'-martensite transforms into austenite [16]. The most significant contribution to the thermal effect in DB is the burnishing velocity [37].

The strain-hardening effect is a consequence of the large surface-equivalent plastic deformation in the DB process. Thus, the surface microhardness increases, and useful residual compressive stresses are generated at a significant depth from the surface layer. Then, the phase transformation $\gamma \rightarrow \alpha'$ occurs. The burnishing force and feed rate contribute most to this mechanical effect. As the burnishing force increases, the equivalent plastic deformation in the surface and near-subsurface layers increases. However, above a certain burnishing force value, the maximum compressive residual stress shifts below the surface layer [16]. A decreased feed rate increases the cyclic loading coefficient (CLC) [38] which is a measure of the accumulated plastic deformation in the surface layer due to DB. A larger CLC yields a greater equivalent plastic deformation of the surface layer and a higher percentage of induced α'-martensite. Combinations of various magnitudes of the DB governing factors change the ratio between the two effects (thermal and mechanical), leading to different SI characteristics, including surface residual stresses and α'-martensite.

In the regression model (2), the absolute values of the dimensionless coefficients b_i and b_{ii} (Table 5) measure the degree of influence of the respective variable x_i on the objective function Y_σ. Of the three variables (x_i), the burnishing force is assumed to have the weakest influence on Y_σ because the coefficients x_1 and x_{11} have relatively small absolute values. The absolute values of the coefficients $b_{ij}, i \neq j$ in front of the mixed products $x_i x_j$ of the variables quantitatively measure the degree of significance of interactions between these variables.

The interaction between the feed rate and burnishing velocity is negligible because the coefficient b_{23} in the regression model (2) is ignored as a minimal quantity. However, the burnishing force interactions with the feed rate and the burnishing velocity cannot be ignored because they are commensurate with the degree of influence of the burnishing force on Y_σ. The physical interaction $x_1 x_2$ is expressed in the synergy between the burnishing force and feed rate in terms of the mechanical effect (e.g., with increasing burnishing force and decreasing feed rate, the CLC increases, that is, the amount of accumulated plastic deformation in the surface layer increases) [38]. Thus, the mechanical effect prevails over the thermal one.

Similarly, the interaction $x_1 x_3$ is expressed in the synergy between the burnishing force and burnishing velocity in terms of the thermal effect. The simultaneous increase in the burnishing force and burnishing velocity increases the power of the frictional forces, generating a greater amount of heat. The more heat generated in the DB process, the more induced

martensite content, decreasing the absolute values of the surface residual stresses measured for both phases (austenitic and martensitic). Thus, the thermal effect prevails over the mechanical one.

Assessing which of the three governing factors dominates is difficult using the method of comparing coefficients. An analysis of variance (ANOVA) was conducted to answer this question. Figure 3 illustrates the significance (degree of influence) of the three driving factors on ESRS. The most significant governing factor is the burnishing velocity, and the burnishing force has the least influence on ESRS. When the three factors are maintained at a lower level (i.e., –1), the ESRS has a maximum absolute value. The reason that the thermal effect is minimal is because the heat generated is minimal; when the burnishing velocity and force are minimal, the power from the frictional forces and the generated heat are minimal. When the feed rate is maintained at a lower level, the CLC [38] is maximal (i.e., more equivalent plastic deformation accumulates in the surface layer, which is a prerequisite for increasing residual surface stresses).

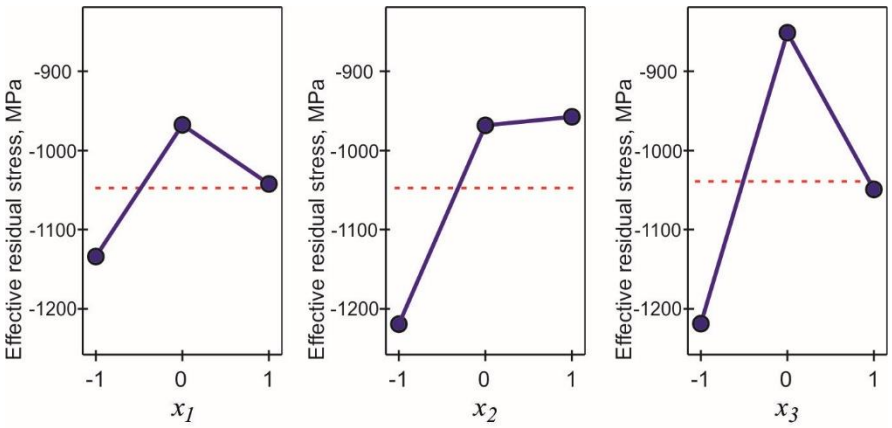

Figure 3.
ANOVA main effects.

The following formula presents the correlation between the dimensionless x_i and physical $\tilde{x}_i$ variables:

$$x_i = \frac{\left(\tilde{x}_i - \tilde{x}_{i,0}\right)}{\left(\tilde{x}_{i,max} - \tilde{x}_{i,0}\right)}, \quad (3)$$

where $\tilde{x}_{i,0}$ and $\tilde{x}_{i,max}$ denote the average and maximum values of the physical variable, respectively.

Substituting (3) into (2) yields the dependence of the hypersurface Y_σ on the physical variables (the three governing factors). Figures 4, 5, and 6 illustrate the dependence of Y_σ on the burnishing force, feed rate, and burnishing velocity, respectively.

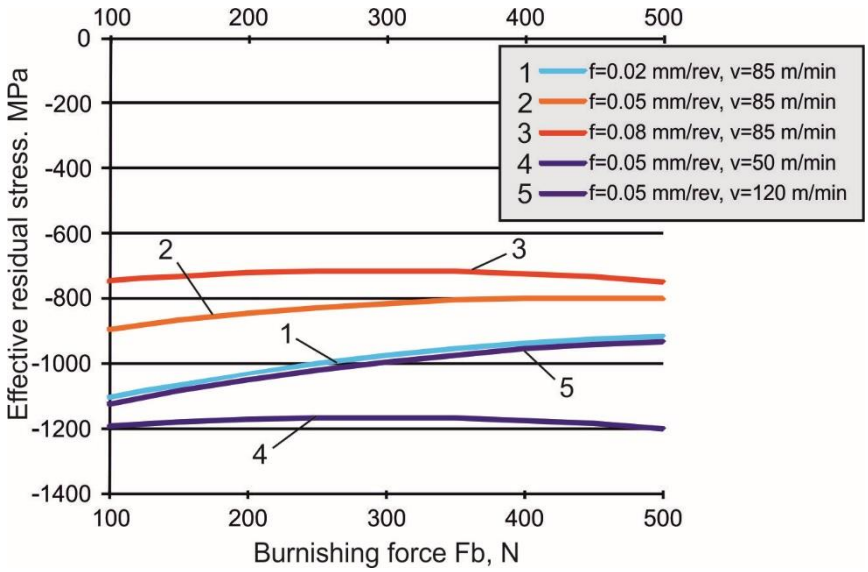

Figure 4.
Dependence of the effective stress on the burnishing force.

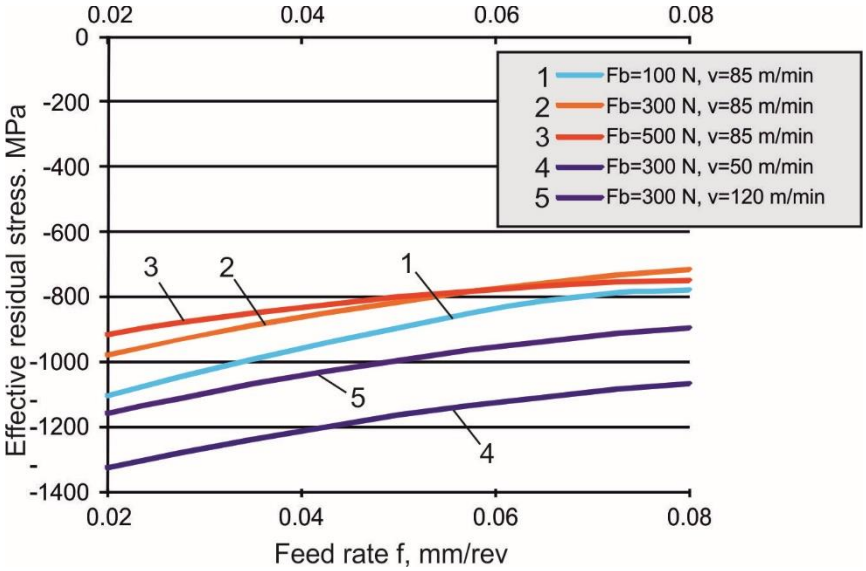

Figure 5.
Dependence of the effective stress on the feed rate.

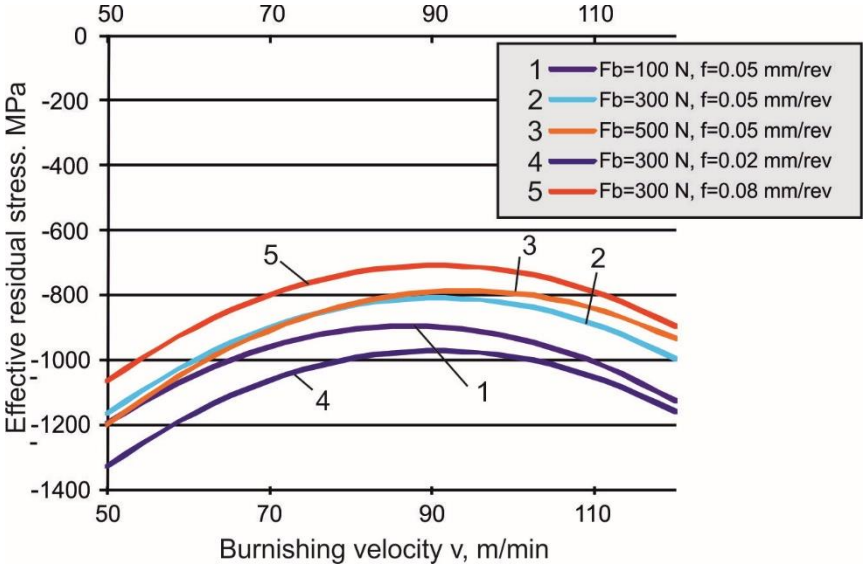

Figure 6.
Dependence of the effective stress on the burnishing velocity.

Figure 4 confirms the conclusion above that the burnishing force has the weakest influence on the effective residual stress. When the feed rate and burnishing velocity are constant, the change in the burnishing force affects strain-hardening (i.e., the mechanical effect) and the thermal effect. Increasing the burnishing force increases the degree of strain-hardening, increasing residual surface stresses (for both phases). However, further increases in the burnishing force increase the depth of the compression zone and shift the maximum compressive stress below the surface layer [16] (i.e., decreasing the surface residual stress). With an increasing burnishing force, the friction forces increase, the power of these forces increases, and the amount of heat generated increases. Increased heat leads to a softening effect and suppresses the $\gamma \rightarrow \alpha'$ transformation, leading to the reverse transformation $\alpha' \rightarrow \gamma$ of the formed martensite. Thus, the absolute values of the residual compressive stresses in the surface layer decrease. Therefore, the two effects (mechanical and thermal) act in opposite directions, and the change in ESRS is minimal.

At a constant burnishing force and velocity, the feed rate affects the ESRS unidirectionally (Figure 5); increasing the feed rate decreases the absolute value of the ESRS. This steady trend is a direct consequence of the fact that the feed rate (by itself) does not create a thermal effect. A lower feed rate results in a greater overlapping effect and greater CLC [38]. Thus, equivalent plastic deformation in the surface layer accumulates, and the amount of strain-induced martensite (i.e., $\gamma \rightarrow \alpha'$ transformation is accelerated) increases. Moreover, the absolute value of ESRS increases.

Unlike the feed rate, the influence of the burnishing velocity is not unidirectional (Figure 6). At a constant burnishing velocity and feed rate, changing the burnishing velocity creates mechanical and thermal effects. With an increasing burnishing velocity, the strain velocity (mechanical effect) increases, and with an increased strain velocity, the yield strength of the metal increases, approaching the ultimate tensile stress (i.e., the relative strength of the surface layer increases at the expense of reduced plasticity). Moreover, with an increasing burnishing velocity, the amount of generated

heat increases, causing a softening effect [37] including a decrease in strain-induced α'-martensite. The ratio between the two effects (mechanical and thermal) determines the magnitude of the ESRS (at a constant burnishing force and feed rate).

The physical characteristics of SI (surface microhardness, percentage of induced martensite, and ESRS) have a common physical basis: the interaction between mechanical and thermal effects. Based on the numerical values of the three SI characteristics in Table 4 and 6, this work obtains the following linear model of the dependence of the ESRS on the microhardness and the percentage of induced α'-martensite in the surface layer:

$$ES = -1887.3397 + 2.0098444\ HV - 7.2385356\ M, \quad (4)$$

where ES denotes the effective residual stress, HV represents the microhardness, and M indicates the percentage of content of α'-martensite.

Table 6.
Surface microhardness.

Experimental point	1	2	3	4	5	6	7	8	9	10	11	12	13	14
Microhardness HV	595	658	523	590	554	590	488	554	534	590	585	539	598	551

Figure 7 presents the graphical visualization of the model (4). The ESRS depends on the percentage of content of the induced martensite to a greater extent than the surface microhardness.

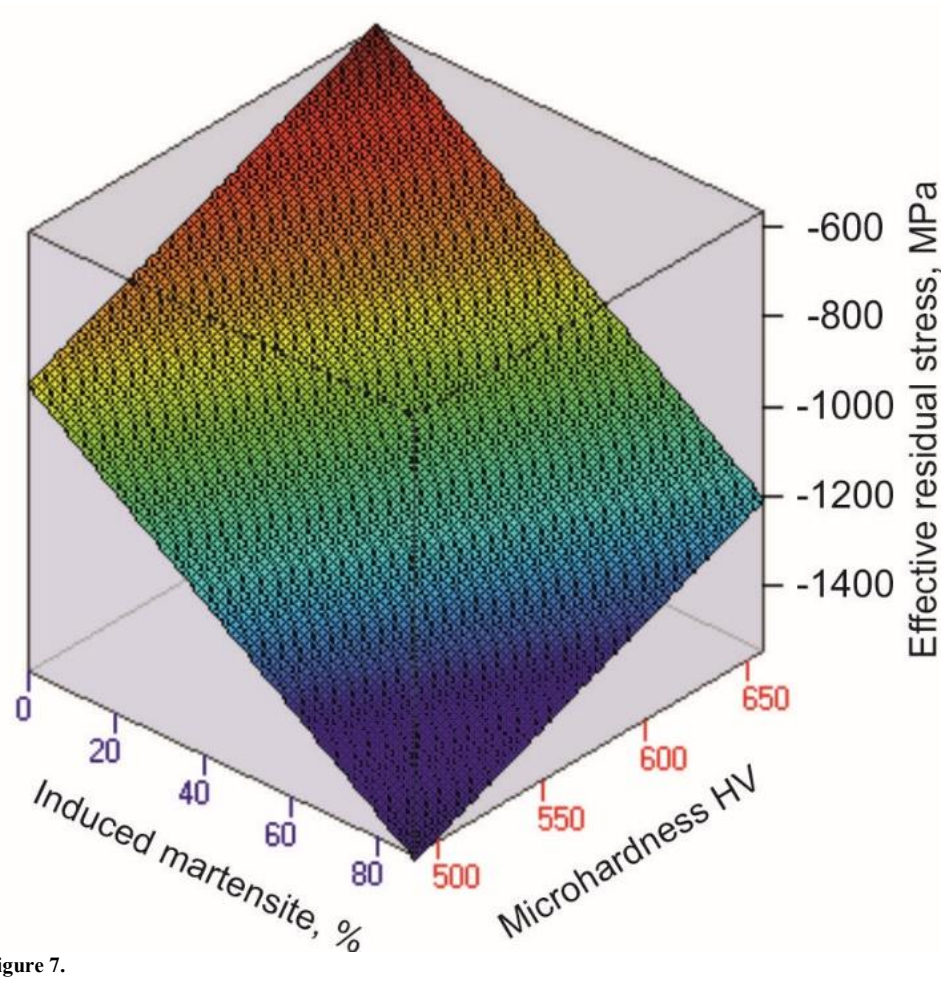

Figure 7.
Dependence of the effective residual stress on the microhardness and the percentage content of induced martensite.

5. Conclusions

The DB method induces α'-martensite in the surface layers of AISI 304 steel specimens in different proportions with austenite, depending on the magnitudes of the governing factors. The presence of two phases in the surface layer creates a problem when measuring the surface residual stresses using the X-ray diffraction technique regarding the phase in which the elastic constants should be chosen. This study introduces the concept of ESRS to solve this problem. The ESRS is the sum of the measured residual stresses for these two phases, multiplied by the respective weighting factors corresponding to the percentage of content of the two phases. Thus, the inhomogeneous surface (according to the phase composition criterion) is homogenized, and the ESRS is a characteristic of this homogenized surface. The significant new findings concerning the nature of the DB process are as follows:

- This work presents a mathematical model of the ECPC depending on the burnishing force, feed rate, and burnishing velocity.

- Of the three governing factors, the most significant is the burnishing velocity, and the least important is the burnishing force.
- The DB method produces two effects: mechanical and thermal. Combinations of various magnitudes of the DB governing factors change the ratio between the two effects, leading to different SI characteristics, including surface residual stresses and α'-martensite.
- The feed rate effect on ESRS is unidirectional: The absolute value of ESRS decreases as the feed rate increases. This sustainable trend is a direct consequence of the fact that the feed rate does not create a thermal effect. Conversely, the burnishing force and velocity influence the mechanical and thermal effects created by DB.
- The ESRS depends on the percentage of induced martensite to a greater extent than the surface microhardness.

6. Limitations and Future Research

The validity of the results, discussion, and conclusions is limited by the selected governing factors and their variation intervals. The results provide grounds for continuing this research with the inclusion of two more governing factors (the radius of the diamond insert and number of passes) and under various burnishing conditions (lubrication, cooling, etc.).

Abbreviations:

ANOVA	Analysis of variance
CNASS	Chromium-nickel austenitic stainless steel
CLC	Cyclic loading coefficient
DB	Diamond burnishing
ESRS	Effective surface residual stress
SI	Surface integrity

References

[1] Grand View Research Company, "Stainless steel market size, share & trends analysis report by grade (300 series, duplex series), by product (flat, long), by application (building & construction, consumer goods), by region, and segment forecast, 2024–2030," Report ID: 9781680389456), 2024.

[2] G. Duncheva and J. Maximov, "Cold working technologies for increasing the fatigue life of metal structural components with fastener holes—review and perspectives," *The International Journal of Advanced Manufacturing Technology,* vol. 136, no. 7, pp. 2909-2943, 2025. https://doi.org/10.1007/s00170-025-15020-0

[3] J. Maximov, G. Duncheva, A. Anchev, V. Dunchev, Y. Argirov, and M. Nikolova, "Effects of heat treatment and diamond burnishing on fatigue behaviour and corrosion resistance of AISI 304 austenitic stainless steel," *Applied Sciences,* vol. 13, no. 4, p. 2570, 2023. https://doi.org/10.3390/app13042570

[4] G. Jagadeesh and S. Gangi Setti, "A review on latest trends in ball and roller burnishing processes for enhancing surface finish," *Advances in Materials and Processing Technologies,* vol. 8, no. 4, pp. 4499-4523, 2022. https://doi.org/10.1080/2374068X.2022.2077534

[5] G. Duncheva, J. Maximov, V. Dunchev, A. Anchev, T. Atanasov, and J. Capek, "Single toroidal roller burnishing of 2024-T3 Al alloy implemented as mixed burnishing process," *The International Journal of Advanced Manufacturing Technology,* vol. 111, no. 11, pp. 3559-3570, 2020. https://doi.org/10.1007/s00170-020-06350-2

[6] J. Maximov and G. Duncheva, "Finite element analysis and optimization of spherical motion burnishing of low-alloy steel," *Proceedings of the Institution of Mechanical Engineers, Part C: Journal of Mechanical Engineering Science,* vol. 226, no. 1, pp. 161-176, 2012. https://doi.org/10.1177/0954406211412024

[7] M. Korzynski, *Slide diamond burnishing (Nonconventional finishing technologies)*. Warsaw, Poland: Wydawnictwo Naukowe PWN, 2013.

[8] J. T. Maximov, G. V. Duncheva, A. P. Anchev, and V. P. Dunchev, "Slide burnishing versus deep rolling—A comparative analysis," *The International Journal of Advanced Manufacturing Technology,* vol. 110, no. 7, pp. 1923-1939, 2020. https://doi.org/10.1007/s00170-020-05950-2

[9] J. T. Maximov, G. V. Duncheva, A. P. Anchev, and V. P. Dunchev, "Smoothing, deep, or mixed diamond burnishing of low-alloy steel components–optimization procedures," *The International Journal of Advanced Manufacturing Technology,* vol. 106, no. 5, pp. 1917-1929, 2020. https://doi.org/10.1007/s00170-019-04747-2

[10] J. Zaghal, V. Molnár, and M. Benke, "Improving surface integrity by optimizing slide diamond burnishing parameters after hard turning of 42CrMo4 steel," *The International Journal of Advanced Manufacturing Technology,* vol. 128, no. 5, pp. 2087-2103, 2023. https://doi.org/10.1007/s00170-023-12008-6

[11] A. Skoczylas, K. Zaleski, and J. Matuszak, "Evaluation of the effectiveness of surface defect removal by slide burnishing," *Applied Sciences,* vol. 15, no. 13, p. 7398, 2025. https://doi.org/10.3390/app15137398

[12] F. T. Kebede, C. Felho, and I. Sztankovics, "Improving surface roughness of 42CrMo4 low alloy steel shafts by applying varying feed in the multi-pass slide burnishing process," *Applied Sciences,* vol. 15, no. 16, p. 9063, 2025. https://doi.org/10.3390/app15169063

[13] D. Toboła and B. Kania, "Phase composition and stress state in the surface layers of burnished and gas nitrided Sverker 21 and Vanadis 6 tool steels," *Surface and Coatings Technology,* vol. 353, pp. 105-115, 2018. https://doi.org/10.1016/j.surfcoat.2018.08.055

[14] D. Toboła and A. Łętocha, "Influence of combined mechanical processes on tribological properties of tool steels Vanadis 8 and vancron 40 with a similar hardness," *Frontiers in Mechanical Engineering,* vol. 7, p. 775059, 2021. https://doi.org/10.3389/fmech.2021.775059

[15] D. Toboła, "Influence of sequential surface treatment processes on tribological performance of vanadis 6 cold work tool steel," *Wear,* vol. 488–489, p. 204106, 2022. https://doi.org/10.1016/j.wear.2021.204106

[16] J. Maximov, G. Duncheva, A. Anchev, V. Dunchev, and Y. Argirov, "Effect of diamond burnishing on fatigue behaviour of AISI 304 chromium-nickel austenitic stainless steel," *Materials,* vol. 15, no. 14, p. 4768, 2022. https://doi.org/10.3390/ma15144768

[17] S. Smolnicki and G. Varga, "Analysis of surface roughness of diamond-burnished surfaces using Kraljic matrices and experimental design," *Applied Sciences,* vol. 15, no. 14, p. 8025, 2025. https://doi.org/10.3390/app15148025

[18] J. Maximov, G. Duncheva, A. Anchev, and V. Dunchev, "Explicit correlation between surface integrity and fatigue limit of surface cold worked chromium-nickel austenitic stainless steels," *The International Journal of Advanced Manufacturing Technology,* vol. 133, pp. 6041-6058, 2024.

[19] Y. Argirov, J. Maximov, G. Duncheva, A. Anchev, V. Dunchev, and T. Mechkarova, "Evolution of surface integrity characteristics and mechanical behavior of diamond burnished and turned AISI 304 steel specimens after prolonged exposure to natural seawater," *Coatings,* vol. 15, no. 1, p. 31, 2025. https://doi.org/10.3390/coatings15010031

[20] D. Toboła, J. Morgiel, and Ł. Maj, "TEM analysis of surface layer of Ti-6Al-4V ELI alloy after slide burnishing and low-temperature gas nitriding," *Applied Surface Science,* vol. 515, p. 145942, 2020. https://doi.org/10.1016/j.apsusc.2020.145942

[21] G. V. Duncheva, J. T. Maximov, A. P. Anchev, V. P. Dunchev, and Y. B. Argirov, "Multi-objective optimization of the internal diamond burnishing process," *Materials and Manufacturing Processes,* vol. 37, no. 4, pp. 428-436, 2022. https://doi.org/10.1080/10426914.2021.1981937

[22] J. Maximov and G. Duncheva, "Effects of cryogenic-and cool-assisted burnishing on the surface integrity and operating behavior of metal components: A review and perspectives," *Machines,* vol. 12, no. 5, p. 312, 2024. https://doi.org/10.3390/machines12050312

[23] J. Maximov and G. Duncheva, "Effects of diamond burnishing on surface integrity, fatigue, wear, and corrosion of metal components—review and perspectives," *The International Journal of Advanced Manufacturing Technology,* vol. 139, pp. 4233–4267, 2025. https://doi.org/10.1007/s00170-025-16158-7

[24] D. Toboła *et al.*, "Microstructural dependence of tribological properties of Ti-6Al-4V ELI alloy after slide burnishing/shot peening and low-temperature gas nitriding," *Surface and Coatings Technology,* vol. 501, p. 131941, 2025. https://doi.org/10.1016/j.surfcoat.2025.131941

[25] J. Maximov, G. Duncheva, A. Anchev, V. Dunchev, and Y. Argirov, "Improvement in fatigue strength of chromium–nickel austenitic stainless steels via diamond burnishing and subsequent low-temperature gas nitriding," *Applied Sciences,* vol. 14, no. 3, p. 1020, 2024. https://doi.org/10.3390/app14031020

[26] G. Varga and V. Ferencsik, "Experimental examination of surface micro-hardness improvement ratio in burnishing of external cylindrical workpieces," *Cutting & Tools in Technological Systems,* vol. 93, pp. 114–121, 2020. http://dx.doi.org/10.20998/2078-7405.2020.93.13

[27] M. Okada *et al.*, "Development and characterization of diamond tip burnishing with a rotary tool," *Journal of Materials Processing Technology,* vol. 244, pp. 106-115, 2017. https://doi.org/10.1016/j.jmatprotec.2017.01.020

[28] A. Skoczylas, K. Zaleski, J. Matuszak, K. Ciecieląg, R. Zaleski, and M. Gorgol, "Influence of slide burnishing parameters on the surface layer properties of stainless steel and mean positron lifetime," *Materials,* vol. 15, no. 22, p. 8131, 2022. https://doi.org/10.3390/ma15228131

[29] P. L. Mangonon and G. Thomas, "Structure and properties of thermal-mechanically treated 304 stainless steel," *Metallurgical Transactions,* vol. 1, no. 6, pp. 1587-1594, 1970. https://doi.org/10.1007/BF02642004

[30] M. Mhaede and L. Wagner, "Effect of austenite stability on phase transformation and fatigue performance of stainless steels after various mechanical surface treatment," presented at the 11th International Conference on Shot Peening, At: South Band, Indiana, USA, 2011.

[31] I. Nikitin, I. Altenberger, and B. Scholtes, "Effect of deep rolling at elevated and low temperatures on the isothermal fatigue behavior of AISI 304," in *Proceedings of 9th International Conference on Shot Peening, Paris*, 2005, pp. 185-190.

[32] M. Ichkova, "Effects of diamond burnishing process parameters on the surface roughness of AISI 304 austenitic stainless steel," *Edelweiss Applied Science and Technology,* vol. 9, no. 4, pp. 1075-1087, 2025. https://doi.org/10.55214/25768484.v9i4.6174

[33] ISO, *ISO 6892-1:2019 - Metallic materials - Tensile Testing - Part1: Method of test at room temperature*. Switzerland, Geneva: ISO, 2019.

[34] DiffracDquant, *Quantitative analysis from calibration to reporting*. Bruker AXS GmbH: Germany, Karlsrue, 2018.

[35] G. E. Box and K. B. Wilson, *On the experimental attainment of optimum conditions. In Breakthroughs in statistics: Methodology and distribution*. New York: Springer, 1992.

[36] I. N. Vuchkov and I. I. Vuchkov, *QStatLab Professional, v. 6.1.1.3 - statistical quality control software*. Bulgaria: Sofia: User's Manual, 2009.

[37] J. Maximov, G. Duncheva, A. Anchev, N. Ganev, I. Amudjev, and V. Dunchev, "Effect of slide burnishing method on the surface integrity of AISI 316Ti chromium–nickel steel," *Journal of the Brazilian Society of Mechanical Sciences and Engineering,* vol. 40, no. 4, p. 194, 2018. https://doi.org/10.1007/s40430-018-1135-3

[38] J. Maximov, G. Duncheva, A. Anchev, N. Ganev, and V. Dunchev, "Effect of cyclic hardening on fatigue performance of slide burnished components made of low-alloy medium carbon steel," *Fatigue & Fracture of Engineering Materials & Structures,* vol. 42, no. 6, pp. 1414-1425, 2019. https://doi.org/10.1111/ffe.13001